Giant, 17, 2024, 100228

Full-length article

Directing and reconfiguring colloidal assembly by disclination networks in nematic liquid crystal as templates

Yubing Guo[a,b,1], **Miao Jiang**[a,c,1], **Sajedeh Afghah**[a], **Chenghui Peng**[a], **Robin L.B. Selinger**[a,d], **Oleg D. Lavrentovich**[a,d], **Qi-Huo Wei**[c,e,*]

[a] Advanced Materials and Liquid Crystal Institute, Kent State University, Kent, OH, USA
[b] School of Medical Technology, Beijing Institute of Technology, Beijing, China
[c] Department of Mechanical and Energy Engineering, Southern University of Science and Technology, Shenzhen, China
[d] Department of Physics, Kent State University, Kent, OH, USA
[e] Center for Complex Flows and Soft Matter Research, Southern University of Science and Technology, Shenzhen, China

Keywords: Topological defects, Self-assembly, Photopatterning, Optical reconfiguration

Exotic structures with interesting physical and chemical properties can be achieved by self-organizing engineered building blocks. The central aim for self-assembly is to precisely control the position and orientation of individual building blocks. In this work, we use topological defects (disclinations) in nematic liquid crystals as templates to direct the self-assembly of colloidal particles into designable 3D structures. By photopatterning preprogrammed molecular orientations at two confining surfaces, we created pre-designable disclination networks and characterized their interactions with spherical colloidal particles. We find that colloidal particles are attracted to different disclinations depending on the orientation of the point defect (elastic dipole) around the colloids. We demonstrate that the positions, network structures, and orientation of the elastic dipoles of the colloidal chains can be pre-designed and reconfigured with remote illumination of polarized light.

1 Introduction

Self-assembly enables building new structures and materials from bottom up with engineered building units. By designing chemical compositions and physical properties of these building units, materials with exotic properties that do not exist in nature may be obtained [1–3]. The structures of self-assembled materials are determined primarily by the interactions between these building units and can be controlled by their geometric shapes, surface properties and dispersing media. Liquid crystals, characterized by their long-range molecular orientational ordering and liquid-like flow properties, are an intriguing dispersing medium for self-assembly. In contrast to isotropic media such as water, liquid crystals offer high flexibility in controlling not only interactions but also transport and placements of the particles [4–6]. Self-assembly of colloidal particles in liquid crystals with uniform molecular orientation already yields various interesting structures, such as linear chains, two-dimensional (2D) and three-dimensional (3D) crystals that are often wrapped by topological defect lines [4,6–12]. The interactions between the particles due to elastic distortion of the director field can be further enriched by introducing non-uniform liquid crystal molecular orientations

* Corresponding author at: Department of Mechanical and Energy Engineering, Southern University of Science and Technology, Shenzhen, China.
E-mail address: weiqh@sustech.edu.cn (Q.-H. Wei).
Received 16 August 2023; Received in revised form 18 December 2023; Accepted 19 December 2023
[1] These authors contributed equally.

https://doi.org/10.1016/j.giant.2023.100228

[6,13] or employing particles with complex topological shapes [14–18]. Additionally, the interplay between elastic forces and other forces such as magnetic or electro-static forces can lead to complex colloidal structures such as both positionally and orientationally ordered triclinic lattices of nanorods [13,19]. An important advantage of liquid crystals as a medium for guiding colloidal self-assembly is related to the long-range repulsion between colloids and the bounding substrates, or the effect of elastic "levitation" that can mitigate gravity-favored sedimentation [20].

One ultimate goal of the self-assembly is to precisely control the location and orientation of individual particles, to assemble, disassemble and reconfigure complex while designable structures. Many of these desired capabilities can be realized by using liquid crystals as the dispersing medium. By using spatially non-uniform molecular director fields generated by wavy boundaries, it has been demonstrated that colloidal particles can be placed into predesigned locations by a "lock-and-key" type of particle-wall interactions [21]. In an alternate approach, predesigned complex surface anchoring patterns inscribed via a photopatterning technique [22–24] provide a versatile way to direct particles into positions and orientations based on their surface anchoring and geometric shapes [6,25]. For example, it was shown that colloidal spheres with homeotropic (perpendicular) surface anchoring are driven by the director patterns into areas with splay deformation, while spheres with planar (tangential) surface anchoring are driven into areas with bend deformation [6]. Topological defects, including point and line defects such as disclination lines and disclination loops, exhibit a great potential as templates for attracting and assembling particles of nanometers to micrometers in size [5,13,26–35]. Notably, a recent work by Abbott and coworkers has pushed the defect-mediated self-assembly down to the molecular level [36]. Several techniques have been used to generate and reconfigure topological defects [5,7,13,22,26,29,31,32,37–39], via micro-fabricated pyramid and pillar arrays [29,32] or suspended colloidal particles [5,7,26], or flat confining surfaces with complex director fields by photoalignments [13,22,31] or mechanical rubbing [39]. These studies demonstrate many appealing features of topological defects as templates for self-assembly, while triggering a question whether the approach can be developed further to achieve more complex geometries of assembly and especially to introduce the new feature of reconfigurability.

Here, we present a versatile approach to design, generate, and reconfigure disclination networks by a plasmonic photopatterning technique and use these disclinations as templates to control and reconfigure positions, network structures, and elastic dipole directions of colloidal particles. We measure the interaction potentials between the dislocations and colloidal particles with homeotropic (perpendicular) surface anchoring, and find that the colloidal particles are trapped by the disclinations with local molecular orientations aligned with the colloidal particles' elastic dipole orientation. We demonstrate that the colloidal particles can self-assemble into designed positions with pre-determined elastic dipole directions set by the disclination templates, and that these self-assembled colloidal structures can be reconfigured remotely by illuminating the samples with linearly polarized light.

2 Results and discussion

2.1 Design and generation of disclination networks

We designed liquid crystal cells with uniform planar alignment at the top surface and a planar director pattern of topological point defect arrays at the bottom surface. We denote the orientation angle of the director with respect to the x-axis at the top and bottom surfaces as $\psi_t(x,\ y)$ and $\psi_b(x,\ y)$, respectively. The director fields for the periodic topological defect arrays are obtained by tiling square patches where each patch contains one topological defect at its center $(x_0,\ y_0)$ with a director field described by $\psi_b(x,\ y) = s\varphi(x,\ y) + \psi_0$, where the polar angle $\varphi(x,y) = tan^{-1}\frac{y-y_0}{x-x_0}$, s is the defect charge and ψ_0 is the initial angle when the polar angle is 0.

As an example to illustrate how to generate disclination networks, we use $+1/2$ and $-1/2$ topological defect arrays at the bottom substrate. To make sure that the azimuthal angle is a smooth function at the boundaries between neighboring square patches, we need to have $\psi_{0L}=\pi/4$, and $\psi_{0R}=-\pi/4$ for $\pm1/2$ defect arrays, where ψ_{0L} *and* ψ_{0R} represent the initial angle for the two defects on the left and the initial angle for the two defects on the right respectively. The liquid crystal cells were prepared with a $\sim$30 μm gap between the top and bottom surfaces, and the liquid crystal used is the 4-Cyano-4′-pentylbiphenyl (5CB). When $\psi_t(x,\ y) = 0^\circ$ (Fig. 1a), disclinations emerge from the $+1/2$ and $-1/2$ point defects (marked as circles and diamonds respectively, Fig. 1b) and connect two neighboring $+1/2$ and $-1/2$ defects. The fact that each disclination connects $a\ +\ 1/2$ point defect to a $-1/2$ point defect reflects the well-known topological equivalence between them in the three-dimensional (3D) order parameter space, or the director around the disclination could be transformed continuously from one into one another [40,41]. These twist disclinations are located close to the path with $\psi_b(x,\ y) = 90^\circ$, or the boundary between the regions of opposite twists in the vertical direction, i.e. $(x = L/4,\ \ y \subset [0, L/4] \cup [3L/4, L])$ or $(x = 3L/4,\ \ y \subset [0, L/4] \cup [3L/4, L])$ where L denotes one period of the pattern size as indicated in Fig. 1a. The director field at the bottom surface exhibits predominantly a splay deformation.

The 3D director fields were obtained by numerical calculations using a GPU-enabled director tensor relaxation algorithm for the minimization of the Frank-Oseen Free Energy [42]. To compare the numerical results with the experimental observations, we calculated the POM images of these simulated director fields by using the Jones matrix method [43], and observed that the calculated POM images are in good agreement with the experiments (Fig. 1c). We can see that the disclinations anchor two ends at the centers of two neighboring $\pm1/2$ defects, in good agreement with experimental observations. The disclinations are about 1/6 of the gap distance above the bottom surface (Fig. 1d).

The disclination networks can be varied by simply changing the orientation of the uniform director at the top surface. For example, for $\psi_t = 90^o$, we obtain a different network of disclinations (Fig. 1f) where the point defects connected by

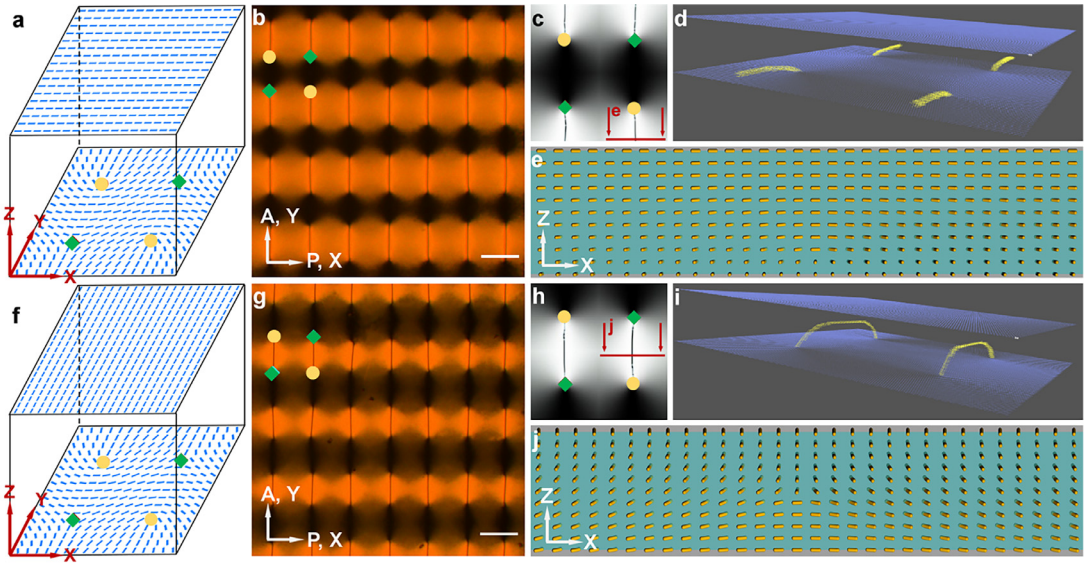

Fig. 1

Exemplary disclination networks generated by $\pm 1/2$ point defect arrays at the bottom substrate. (**a, f**) Schematic of the LC cell geometry with the top surface uniformly aligned along x axis (a) and y axis (f), and the bottom surface patterned into $\pm 1/2$ point defects. The yellow circle and green diamond symbols mark the cores of the $+1/2$ and $-1/2$ points, respectively. (**b, g**) POM images of the LC cells with disclinations formed by surface patterns in (a) and (f). (**c, h**) Simulated POM images of the LC cells with the boundary conditions in (a) and (f). (**d, i**) 3D view of the simulated disclinations in (c) and (h). (**e, j**) Simulated LC director fields in a plane (marked with red lines in c and h) perpendicular to and across the middle point of the disclinations. The red circles show the regions where the disclination cores are located. The scale bars in (b) and (g) are 50 μm.

the disclinations are shifted by one half period along the y-axis (compare Fig. 1b and 1g). Meanwhile, the molecular orientation under the disclination is $\psi_b(x,\ y) = 0^\circ$, around which the director exhibit predominantly bend deformation for ($x = \mathrm{L}/4,\ y \subset [\mathrm{L}/4,\ 3\mathrm{L}/4]$) or ($x = 3\mathrm{L}/4,\ y \subset [\mathrm{L}/4,\ 3\mathrm{L}/4]$). Numerical simulations can well reproduce the experimental POM image (Fig. 1h). A 3D perspective view shows that the disclinations are repelled from the bottom surface with a flat middle section (Fig. 1i). In contrast to the case with $\psi_t(x,\ y) = 0^\circ$, the disclination is located now at the middle of the cell gap, indicating different disclination-surface interactions (Fig. 1j).

The distance between the disclination and the bottom surface is determined by the blance between the surface tension of the disclination and the interaction with the surface (see Ref. [33]). For these two types of disclinations in Fig. 1d and 1i, the director fields at the bottom surface contain a splay deformation and bend deformation, respectively, leading different disclination-surface interactions. In our simulation, the ratio between splay (K_1), twist (K_2), and bend elastic constant (K_3) is around 6:4:9. Therefore, the free energy is higher for the disclinations in Fig. 1i to get close to bottom surface than those in Fig. 1d, which results in higher position of disclinations in Fig. 1i than those in Fig. 1d.

Numerical simulations can show that the z-component of the director is close to zero, indicating that molecules are parallel to the x-y plane, and the directors in the two sides of the disclination rotate from the bottom to the top with opposite twist directions (Fig. 1e and 1j). From the simulated director field (Fig. 1e and 1j), it can also be noted that the director twists uniformly away from the disclination, while twists only near the core region otherwise.

2.2 Interaction between colloidal particles and the disclinations

We measured the interaction potentials between these photopatterned disclinations and colloidal particles by using optical trapping and motion tracking. To minimize the influence of the birefringence on particle trapping, we used a liquid crystal MLC6815 with low birefringence (~ 0.052 at 550 nm wavelength at 25 °C). We used an optical tweezer system with a Verdi V6 green laser (532 nm, 0.3 W) to place particles near these photopatterned disclinations and recorded their motions after release. From the motion trajectories, we calculated the interaction potential difference $\Delta V(x)$ as a function of the distance x between the colloidal particle and the disclination: $\Delta V(x) = \int_{x_1}^{x_1+x} f dx$. Given that the Reynolds number is very low ($\sim 3 \times 10^{-6}$), the elastic force f acting on the particle should be equal to the viscous force: $f = 6\pi R(\eta_\parallel v_\parallel + \eta_\perp v_\perp)$, where R is the particle radius, $v_\parallel$ and $v_\perp$ are the velocities of colloidal particles, $\eta_\parallel$ and $\eta_\perp$ are viscosities [44]. Here the subscripts $\parallel$ and $\perp$ denote the motion directions parallel and perpendicular to the director, respectively. For MLC6815, $\eta_\parallel$ and $\eta_\perp$ are 12 mPa · s and 22 mPa · s, respectively [6]. As an approximation, we use the average viscosity $\eta_a = \frac{\eta_\parallel + 2\eta_\perp}{3}$ to replace $\eta_\parallel$ and $\eta_\perp$.

The director field around a suspended colloidal particle is distorted to match the alignment conditions set by the particle surface. A sphere with homeotropic alignments usually induces a hedgehog point defect with a topological charge of -1 to compensate the topological charge $+1$ of the sphere [4]. As this distorted director field does not fit to the alignment patterns on the confining surfaces, the colloidal particles are repelled from both the top and bottom surfaces, stable in the middle

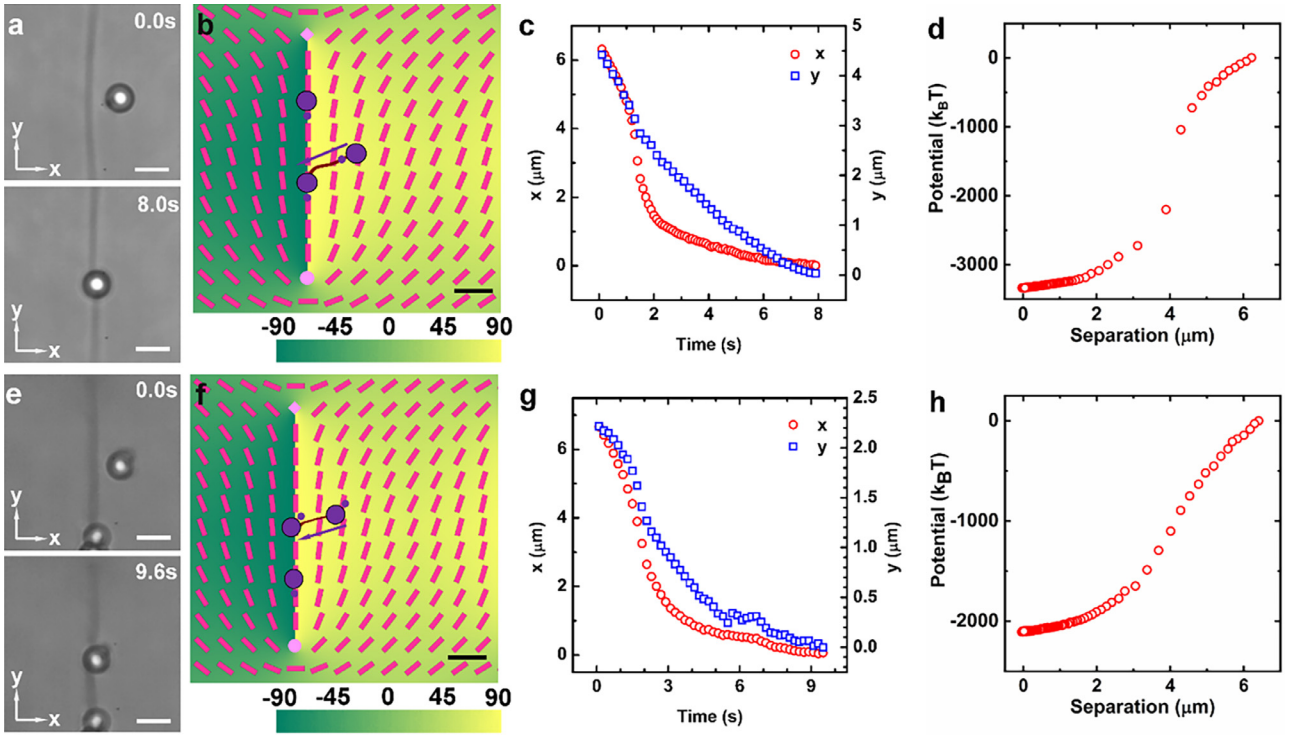

Fig. 2

Interaction between colloidal particles and disclinations in the splay region. (**a, e**) Initial and final position of a particle with a "selected" (a) and "reversed" (e) dipoles. (**b, f**) Trajectory of the particle in (a) and (e). The red bars represent the local director field on the bottom substrate; the background colors represent angle difference of alignment on top surface and bottom surface; the circle and diamond indicates the $+1/2$ and $-1/2$ defect centers. Disclinations appear at location where the twisting angle jumps from -90° to 90° (**c, g**) Relative positions of the particles in x and y directions as a function of time. (**d, h**) Elastic potential differences versus the separation between the colloidal particle and the disclination. The scale bars in panels (a), (b), (e), (f) are 10 μm, 5 μm, 10 μm, and 5 μm, respectively.

of the nematic cell [20]. The hedgehog defect and the colloidal particle form an elastic dipole which can be denoted by a unit vector $\boldsymbol{p}$ from the point defect toward the sphere. It has been shown that $\boldsymbol{p}$ tends to align with director fields to minimize distortions, as theoretically discussed by Lubensky et al. [45] and Lev et al. [46].

In a uniform director field, the elastic dipoles pointing to the two opposite directions of the director have identical elastic energy, and therefore occur with equal probability. While in a non-uniform director field, this inversion symmetry is broken and the elastic dipoles should align along a direction to minimize the total elastic energy [6]. As shown in Fig. 4i, the left particle introduces less deformation than the right one to the original director field, and thus is preferred. Hereafter, we refer to dipoles $\boldsymbol{p}$ matching the director field as "selected" dipoles, while $\boldsymbol{p}$ with mismatched polarity as "reversed" dipoles.

When the top surface alignment is along the x-axis (Fig. 1a), a colloidal particle with the "selected" elastic dipole is attracted to the disclinations with an initial speed $\sim$3 μm/s (Fig. 2a-2c). The binding energy between such a colloidal particle and the disclination is $\sim$3400 k_BT (Fig. 2d), implying that the attraction is very strong. Interestingly, a colloidal particle with the "reversed" elastic dipole may also be attracted to the disclinations (Figs. 2e, f), with a lower binding energy $\sim$2100 k_BT (Figs. 2g, h). The observed sharp change in the interaction potential (Fig. 2d and h) indicates that the attraction force increases firstly and then decreases when the particle is approaching the disclination. A more complete understanding of this interaction potential will require detailed numerical studies on how the director fields evolve with their distance.

When the alignment at the top surface is along the y-axis (Fig. 1f), a colloidal particle with "selected" dipole is attracted by the disclinations (Fig. 3a and b), and moves predominantly along the x-axis with a speed $\sim$ 1μm/s (Fig. 3c). The measured binding energy is $\sim$1000 k_BT (Fig. 3d). It can also be observed that a colloidal sphere with a "reversed" dipole is repelled by the disclination (Fig. 3 e and f) and moves away with smaller speeds along the x-axis (Fig. 3g). The difference in the interaction potential is $\sim$700 k_BT for the separations between 9 μm and 18 μm (Fig. 3h).

The colloid-disclination interactions depend on the orientations of the elastic dipoles with respect to the local director fields. It was shown that colloidal spheres with homeotropic surface alignment are attracted to areas with splay deformation while repelled from areas of bend deformation [6]. Pires and co-workers found that the interaction potential between a colloidal particle with homeotropic alignment and a $-1/2$ disclination is inversely proportional to their separations [47]. Fleury and co-workers used such disclinations as templates to grow 3D microwires [27,28]. The director fields in these cases are effectively 2D, with no director variations in the direction perpendicular to the x-y plane.

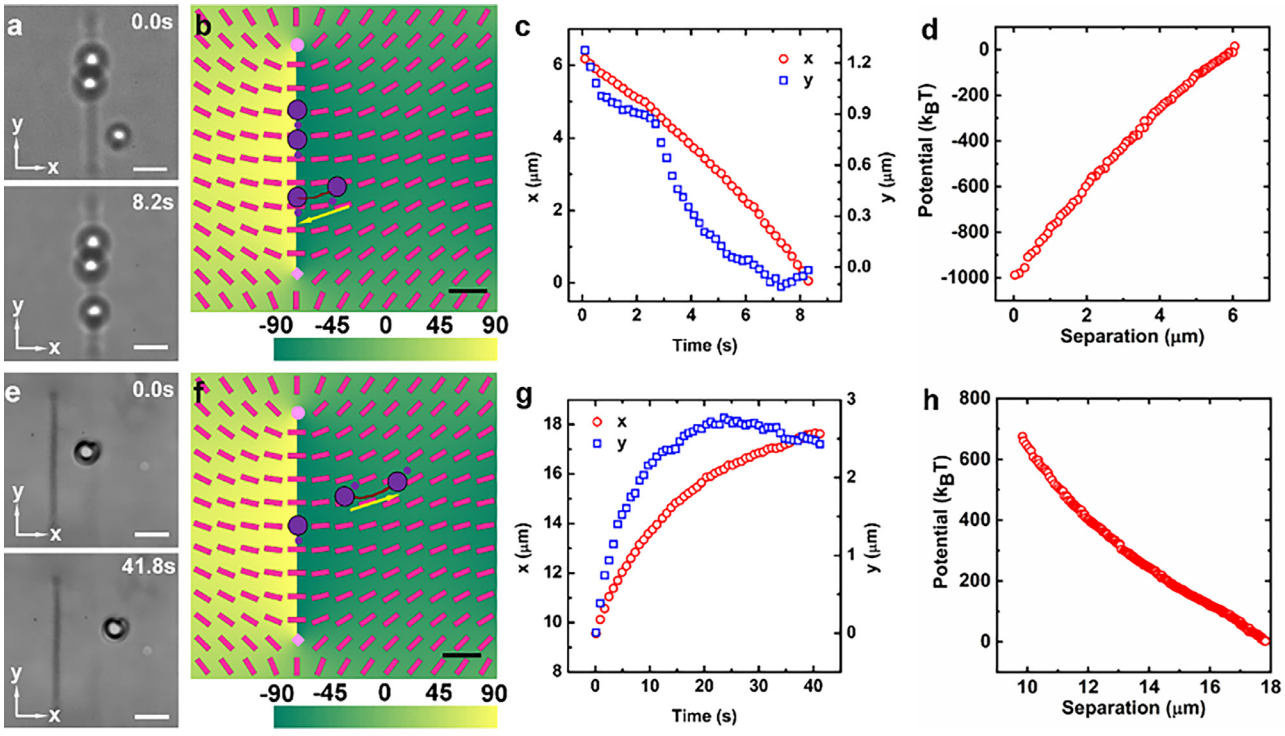

Fig. 3

Interactions between colloidal particles and the disclinations in the bend region. (**a, e**) Initial and final positions of a particle with "selected" (a) and "reversed" (e) dipoles. (**b, f**) Trajectory of a colloidal particle in (a) and (e). The red lines represent the local director field on the bottom substrate; the background colors represent angle difference of alignment on top surface and bottom surface; the $+1/2$ and $-1/2$ defect centers are marked with circle and diamond. Disclinations appear at location where twisting angle jump from -90° to 90° (**c, g**) Positions of the particle in *x* and *y* directions as a function of time. (**d, h**) Elastic potential difference with respect to the separation between the colloidal particle and the disclination. The scale bars in panels (a), (b), (e), (f) are 10 μm, 5 μm, 10 μm, and 5 μm, respectively.

The director fields in our system vary in 3D as schematically shown in Fig. 1a and f. The 3D feature is reflected also in the different heights of the disclinations and colloids. In Fig. 1d and 1i, the disclinations are located at 5 μm or 15 μm from the bottom, while the colloidal particles are at a height $\sim$10 μm as estimated with the theory developed by Pishnyak et al. [20]. Therefore, when colloidal particles are attracted or repelled by the disclination, their motions take place in 3D. While our present measurements track colloid motion only in 2D, it will be interesting to undertake more precise 3D tracking of colloidal particles and 3D mapping of the director field to further elucidate the interactions between colloids and disclinations.

2.3 Templated self-assembly of the colloidal particles

The first system used for templated colloidal assembly consists of liquid crystal cells with a director field of $\pm 1/2$ defect arrays at the bottom surface and a uniform director at the top surface with $\psi_t(x, y) = 0^\circ$, 30°, 60°, and 90°, respectively. The disclination-templated self-assembly is highly effective. All colloidal particles are assembled onto the disclinations, and the elastic dipoles of most spheres point along the same direction with some exceptions of "reversed" dipoles in the splay area (Figs. 4a–d and S2a). These observations demonstrate that colloidal particles can be assembled into predesigned network structures with specified elastic dipole orientations, and into different structures by simply varying the alignment direction at the top surface (Fig. 4a–d). How these "reversed" dipoles can be transferred into "selected" orientations is an interesting question, which might be achieved by locally melting the liquid crystal with high power laser.

The second system consists of liquid crystal cells with ± 1 topological defects at the bottom surface and a uniform director at the top surface, as shown in Fig. 4e–h. We observe a network structures with two disclinations emerging from each defect center. Similarly, almost all the colloidal spheres are attracted onto the disclinations, and on each disclination, the elastic dipoles are arranged in the same direction, forming a polar chain. As shown in Fig. 4g, when the top surface is aligned uniformly along 60°, the disclinations are curved, and the colloidal particles can follow the templates to form curved chains. Consequently, not only the positions of the colloidal spheres but also the shapes of their assemblies can be controlled by designing the liquid crystal molecular orientations at two confining surfaces. We can find that the assembly of colloidal chains causes the radius of curvature of the disclinations to increase. This can be attributed to that the colloid particles tend to form straight chains, as can be seen in Fig. S5. Therefore, the effective line tension of the disclinations is increased by the formation of these colloidal chains.

We measured the average center-to-center distance between two neighboring colloidal particles, which is $\sim$7.2 μm, or about 1.4 times of the particle diameter. This is due to the balance between the attractive force between the head-to-tail elastic dipoles and a shorter-range repulsion between the "-1" hedgehog

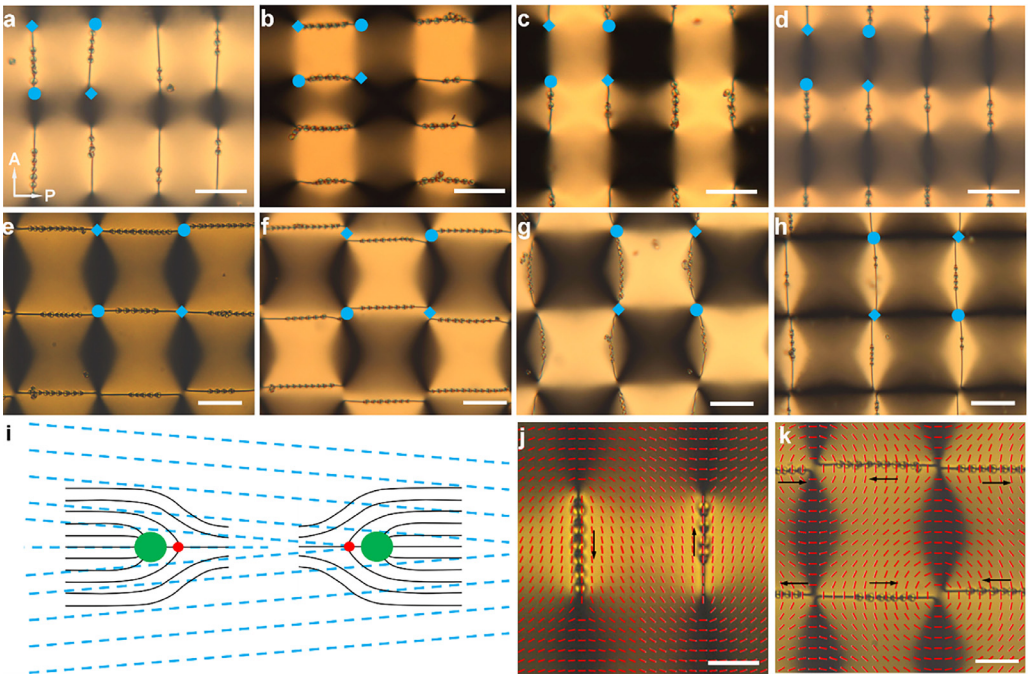

Fig. 4

Disclination templated self-assembly of colloidal particles. (**a-d**) POM images of LC cells with the bottom surfaces patterned with the $\pm 1/2$ point defect arrays, and the top surfaces with uniform planar alignment at $\psi_t = 0°$ (a), 30° (b), 60° (c), and 90° (d). (**e-h**) POM images of LC cells with the bottom surfaces patterned with the ± 1 defect arrays and the top surfaces with uniform planar alignment $\psi_t = 0°$ (e), 30° (f), 60° (g), and 90° (h). (**i**) Colloids with homeotropic surface anchoring in LC with non-uniform molecular orientations. The green sphere corresponds to the colloid while the red sphere correspond to the -1 topological defect. Dashed lines represent the local LC molecular orientations, solid lines represent LC molecular orientations around the colloid. (**j, k**) Self-assembled colloidal chains with designable elastic dipole directions from $\pm 1/2$ defect arrays (j) and ± 1 defect arrays (k). The red bars represent local molecular orientations on bottom surface, and black arrows show elastic dipole direction of each colloidal chain. The scale bars are 50 μm in (a-h), (j) and (k).

of one dipole and the sphere of the neighboring dipole. This ratio of 1.4 between the interparticle distance and the sphere diameter is slightly larger than the value 1.23 obtained from simulations by Fukuda and coworkers [48]. This result implies that the disclination that links the colloids contributes to the repulsive forces along the disclinations. From Fig. 4j and k, we observe that colloidal chains always match their elastic dipole directions with local liquid crystal director field (Fig. 4i). We anticipate that colloidal chains with more complex distributions of elastic dipole directions could be achieved if we use a bottom surface alignment containing defect arrays with higher defect charges (e.g., ± 2).

2.4 Optical reconfiguration of the assembled colloidal structures

These self-assembled colloidal structures can be reconfigured by taking the advantage of the re-writability of the photoalignment material, i.e. the brilliant yellow. The brilliant yellow is a rod-shaped azobenzene molecule that tend to align with its long axis perpendicular to the electrical field (i.e. polarization) of the illuminating light [49]. To make reconfigurable liquid crystal cells, we photopatterned the director field for the topological defects in the brilliant yellow film on the bottom substrate and then spin-coated it with a thin film of the reactive mesogen RM257 mixed with a photoinitiator. The director patterns transferred to the RM257 film were then fixed by photopolymerization with a UV light. The top substrates spin-coated only with the brilliant yellow were photopatterned with uniform alignment.

Fig. 5 presents an example where the bottom surface with the director field of ± 1 defect array is fixed with RM 257 and the top substrate has a uniform director along the y-direction in the brilliant yellow. When the liquid crystal cell was illuminated by light linearly polarized along the y axis, we observed that the disclinations start to bend (Fig. 5b–e) and then reconnect to form new disclinations, changing from the horizontal to vertical connections (Fig. 5f–h). In this process, colloidal particles always follow the disclinations, due to the high binding energy between the colloidal particles and the disclinations. The noise in the optical intensities in the POM images (see Fig. 5c, d, disappeared in Fig. 5e) indicates that the changing molecular orientations during the realignment process are typically inhomogeneous.

We note that colloidal particles can interrupt the reconfiguration process, as shown in the red box in Fig. 5h, where two connected disclinations do not separate to form new disclinations as a result of the presence of colloidal particles. This phenomenon is often observed when the colloidal concentration is high. A complete reconfiguration process with low colloidal concentration of 0.1wt% is shown in Fig. S3. We observed that elastic dipoles are arranged with opposite directions in two neighboring disclinations for ± 1 defect arrays (e.g., Fig. 4e). When these neighboring disclinations meet and reconnect to form new disclinations, elastic dipoles with opposite directions reconfigure to align with approximately the same direction. How assembled colloids with "reversed" dipoles on one disclination

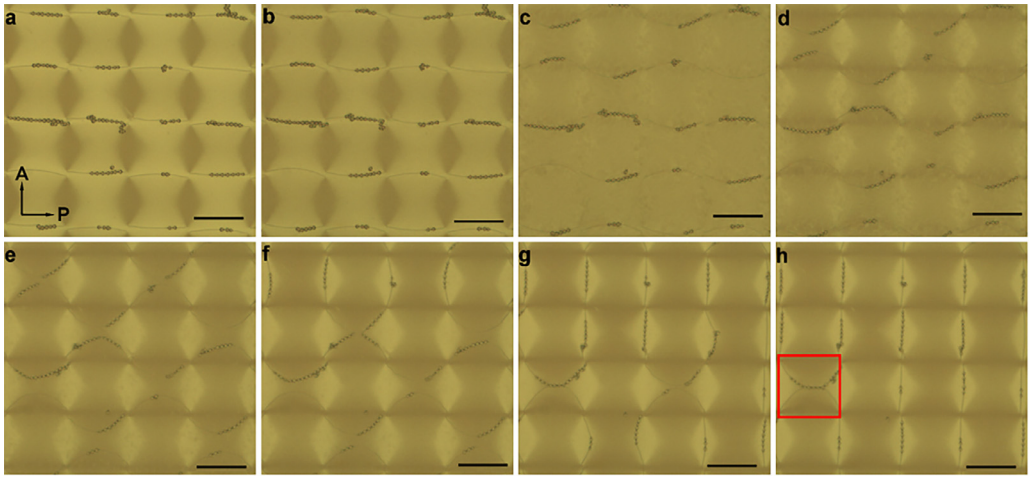

Fig. 5

Remote reconfiguration of the colloidal assembly using linearly polarized light. (**a-h**) POM images of a LC cell after different time of light illuminations: 0 s (a), 30 s (b), 60 s (c), 70 s (d), 77 s (e), 80 s (f), 84 s (g) and 90 s (h). The scale bars in (a-h) are 100 μm.

reorganize during the optical reconfiguration process will be interesting for further studies.

3 Conclusion

To summarize, we demonstrate that the positions, structures, and elastic dipole directions of the template-assembled colloidal particles can be controlled by photopatterning various defect arrays on one surface and manipulating the uniform alignment directions on the other surface, and present an approach to reconfigure them with linearly polarized light. Self-assembly of colloids on disclinations is consistent with interactions between them, which show that colloidal particles tend to be attracted to disclinations with local molecular orientations matching their elastic dipole directions. We expect that the strategy reported in this work will find applications in self-assembly and manipulation of structures with anisotropic properties.

A recent work demonstrated optical reconfiguration of the colloidal assembly by using photopatterned disclinations as templates [50]. Here we show quantitatively how the elastic potentials between the colloidal particles and disclinations depend on their separations, and are influenced by the splay or bend director deformations near the bottom substrates.

4 Materials and methods

4.1 Materials

The 5CB nematic liquid crystal was used in all our experiments for studying disclinations and colloidal assembly. The MLC6815 nematic liquid crystal with low birefringence and low dielectric anisotropy from EM industries was used in the experiments for measuring particle-disclination interactions. Polystyrene (PS) particles with 5 μm diameter (Duke Scientific) were dispersed in a 1 wt% deionized water solution of octadecyl-dimethyl-(3-trimethoxysilylpropyl) ammonium chloride (DMOAP) for 10 h to induce homeotropic surface anchoring. The PS particles coated with DMOAP were centrifuged and washed with deionized water to remove excess DMOAP in the solution, and then dried in an oven at 70 °C for 2 h. The DMOAP-coated particles were then dispersed in 5CB with a concentration of 0.2 wt%, or in MLC6815 with a concentration of 0.05 wt%.

4.2 Liquid crystal cells

Glass substrates were cleaned in an ultrasonic bath with detergents for 15 min, dried in an oven at 90 °C for 10 min, and then cleaned with UV/ozone for 15 min. The cleaned glass substrates were spin-coated with brilliant yellow (0.5 wt% in dimethylformamide) at a 3000 rpm speed for 40 s, and then baked at 95 °C for 30 min to remove the solvent dimethylformamide. The brilliant yellow layers on these glass substrates were photo-patterned by using the plasmonic photopatterning technique as described in our previous paper [22–24]. To form a liquid crystal cell, two substrates with photo-patterned director fields were assembled with the aligning surfaces inside. The cell gaps were controlled using 30 μm fiber spacers. The liquid crystal cells were filled with the colloidal dispersions in the liquid crystal at room temperature.

4.3 Optical reconfiguration

For optical reconfiguration experiments, the molecular director patterns exposed in the photoalignment layers at the bottom substrates were fixed by using photo-polymerizable liquid crystal polymers. After exposure with the plasmonic photopatterning technique, the bottom substrates were coated with a thin layer of RM257 by spin-casting toluene solution containing 10wt% of RM257 (EM industry) and 0.5wt% of Irgacure 651 (Ciba) at 3000 rpm. The substrates were then baked at 50 °C for 3 min and illuminated by non-polarized UV light (365 nm) at an intensity ~1.4 mW/cm^2 for 30 min.

4.4 Numerical simulation

In simulation, the liquid crystal was treated as a continuum medium, described with a director field, $\boldsymbol{n}(x,\ y,\ z)$, which is a univector with $\boldsymbol{n}(x,\ y,\ z) = -\boldsymbol{n}(x,\ y,\ z)$. Liquid crystals were treated as uniaxial and the order parameter is assumed to be spatially uniform. The director field was relaxed to minimize the free energy using a finite difference method. A tensor

representation was used to avoid the mathematic problem in finite differencing of a nematic director field. The boundary condition is periodic on all sides of the cell with fixed patterns on the top and bottom of the cell. Each simulation is initiated differently depending on the patterned substrate. The system size for the numerical simulations is 200 μm × 200 μm × 30 μm, and the mesh size is 0.75 μm in all directions. Splay, twist, and bend elastic constants for the liquid crystals are 6.3pN, 4.0pN, and 9.4pN respectively. Full details of the simulation method are contained in the reference [42].

Declaration of competing interest

The authors declare that they have no known competing financial interests or personal relationships that could have appeared to influence the work reported in this paper.

Data availability

Authors declare that all data supporting the results of this research are available within the manuscript and the Supporting Information. The raw data of this research are available upon request.

CRediT authorship contribution statement

Yubing Guo: Writing – review & editing, Writing – original draft, Visualization, Validation, Methodology, Investigation, Conceptualization. **Miao Jiang:** Writing – review & editing, Writing – original draft, Visualization, Validation, Investigation. **Sajedeh Afghah:** Writing – review & editing, Writing – original draft, Visualization, Validation, Investigation, Formal analysis. **Chenghui Peng:** Writing – original draft, Validation, Investigation. **Robin L.B. Selinger:** Writing – review & editing, Writing – original draft, Visualization, Validation, Supervision, Software, Investigation, Funding acquisition. **Oleg D. Lavrentovich:** Writing – review & editing, Supervision, Resources. **Qi-Huo Wei:** Writing – review & editing, Writing – original draft, Supervision, Project administration, Funding acquisition, Conceptualization.

Acknowledgement

This work at SUSTech was supported by Shenzhen Science and Technology Innovation Committee (GJHZ-20200731095212036), National Natural Science Foundation of China (6210030761 and 12174177). ODL acknowledges the support of the US National Science Foundation grant (DMR-2215191), RLBS acknowledges the support of the US National Science Foundation grant (CMMI-1663041 and CMMI-1436565).

Supplementary materials

Supplementary material associated with this article can be found, in the online version, at doi:10.1016/j.giant.2023.100228.

References

[1] G.M. Whitesides, B. Grzybowski, Self-assembly at all scales, Science 295 (2002) 2418–2421, doi:10.1126/science.1070821.

[2] J.F. Galisteo-lópez, M. Ibisate, R. Sapienza, L.S. Froufe-pérez, A. Blanco, C. Lopez, Self-assembled photonic structures, Adv. Mater. 23 (2011) 30–69, doi:10.1002/adma.201000356.

[3] Y. Mai, A. Eisenberg, Self-assembly of block copolymers, Chem. Soc. Rev. 41 (2012) 5969–5985, doi:10.1039/C2CS35115C.

[4] P. Poulin, H. Stark, T. Lubensky, D. Weitz, Novel colloidal interactions in anisotropic fluids, Science 275 (1997) 1770–1773, doi:10.1126/science.275.5307.1770.

[5] I. Muševič, M. Skarabot, U. Tkalec, M. Ravnik, S. Zumer, Two-dimensional nematic colloidal crystals self-assembled by topological defects, Science 313 (2006) 954–958, doi:10.1126/science.1129660.

[6] C. Peng, T. Turiv, Y. Guo, S.V. Shiyanovskii, Q.H. Wei, O.D Lavrentovich, Control of colloidal placement by modulated molecular orientation in nematic cells, Sci. Adv. 2 (9) (2016) e1600932, doi:10.1126/sciadv.1600932.

[7] A.B. Nych, U.M. Ognysta, V.M. Pergamenshchik, B.I. Lev, V.G. Nazarenko, I. Muševič, M. Škarabot, O.D. Lavrentovich, Coexistence of two colloidal crystals at the nematic-liquid-crystal-air interface, Phys. Rev. Lett. 98 (2007) 057801, doi:10.1103/PhysRevLett.98.057801.

[8] U. Ognysta, A. Nych, V. Nazarenko, M. Skarabot, I. Musevic, Design of 2D binary colloidal crystals in a nematic liquid crystal, Langmuir 25 (2009) 12092, doi:10.1021/la901719t.

[9] A. Nych, U. Ognysta, M. Škarabot, M. Ravnik, S. Žumer, I. Muševič, Assembly and control of 3D nematic dipolar colloidal crystals, Nat. Commun. 4 (2013) 1489, doi:10.1038/ncomms2486.

[10] C. Blanc, D. Coursault, E. Lacaze, Ordering nano- and microparticles assemblies with liquid crystals, Liq. Cryst. Rev. 1 (2013) 83, doi:10.1080/21680396.2013.818515.

[11] M.B. Pandey, T. Porenta, J. Brewer, A. Burkart, S. Čopar, S. Žumer, I.I. Smalyukh, Self-assembly of skyrmion-dressed chiral nematic colloids with tangential anchoring, Phys. Rev. E Stat. Nonlinear, Soft Matter Phys. 89 (6) (2014) 060502, doi:10.1103/PhysRevE.89.060502.

[12] P.J. Ackerman, J. van de Lagemaat, I.I. Smalyukh, Self-assembly and electrostriction of arrays and chains of hopfion particles in chiral liquid crystals, Nat. Commun. 6 (2015) 6012, doi:10.1038/ncomms7012.

[13] H. Yoshida, K. Asakura, J. Fukuda, M. Ozaki, Three-dimensional positioning and control of colloidal objects utilizing engineered liquid crystalline defect networks, Nat. Commun. 6 (2015) 7180, doi:10.1038/ncomms8180.

[14] C.P. Lapointe, T.G. Mason, I.I. Smalyukh, Shape-controlled colloidal interactions in nematic liquid crystals, Science 326 (2009) 1083–1086, doi:10.1126/science.1176587.

[15] M.V. Rasna, K.P. Zuhail, U.V. Ramudu, R. Chandrasekar, J. Dontabhaktuni, S. Dhara, Orientation, interaction and laser assisted self-assembly of organic single-crystal micro-sheets in a nematic liquid crystal, Soft Matter 11 (2015) 7674–7679, doi:10.1039/C5SM01991E.

[16] B. Senyuk, J.S. Evans, P.J. Ackerman, T. Lee, P. Manna, L. Vigderman, E.R. Zubarev, J.Van De Lagemaat, I.I Smalyukh, Shape-dependent oriented trapping and scaffolding of plasmonic nanoparticles by topological defects for self-assembly of colloidal dimers in liquid crystals, Nano Lett 12 (2012) 955, doi:10.1021/nl204030t.

[17] B. Senyuk, Q. Liu, S. He, R.D. Kamien, R.B. Kusner, T.C. Lubensky, I.I. Smalyukh, Topological colloids, N*ature* 493 (2013) 200–205, doi:10.1038/nature11710.

[18] D.V. Sudhakaran, R.K. Pujala, S. Dhara, Orientation dependent interaction and self-assembly of cubic magnetic colloids in a nematic liquid crystal, Adv. Opt. Mater. 8 (2020) 1901585, doi:10.1002/adom.201901585.

[19] H. Mundoor, B. Senyuk, I.I. Smalyukh, Triclinic nematic colloidal crystals from competing elastic and electrostatic interactions, Science 352 (2016) 69–73, doi:10.1126/science.aaf0801.

[20] O.P. Pishnyak, S. Tang, J.R. Kelly, S.V. Shiyanovskii, O.D. Lavrentovich, Levitation, lift, and bidirectional motion of colloidal particles in an electrically driven nematic liquid crystal, Phys. Rev. Lett. 99 (2007) 127802, doi:10.1103/PhysRevLett.99.127802.

[21] Y. Luo, F. Serra, K.J. Stebe, Experimental realization of the "Lock-and-Key" mechanism in liquid crystals, Soft Matter 12 (2016) 6027–6032, doi:10.1039/C6SM00401F.

[22] Y. Guo, M. Jiang, C. Peng, K. Sun, O. Yaroshchuk, O. Lavrentovich, Q.H. Wei, High-resolution and high-throughput plasmonic photopatterning of complex molecular orientations in liquid crystals, Adv. Mater. 28 (2016) 2353–2358, doi:10.1002/adma.201506002.

[23] Y. Guo, M. Jiang, C. Peng, K. Sun, O. Yaroshchuk, O. Lavrentovich, Q.H. Wei, Designs of plasmonic metamasks for photopatterning molecular orientations in liquid crystals, Crystals 7 (2016) 8, doi:10.3390/cryst7010008.

[24] H. Yu, M. Jiang, Y. Guo, T. Turiv, W. Lu, V. Ray, O.D. Lavrentovich, Q.H. Wei, Plasmonic metasurfaces with high UV – Vis transmittance for photopatterning of designer molecular orientations, Adv. Opt. Mater. 7 (2019) 1900117, doi:10.1002/adom.201900117.

[25] C. Peng, T. Turiv, R. Zhang, Y. Guo, S.V. Shiyanovskii, Q.H. Wei, J. de Pablo, O.D Lavrentovich, Controlling placement of nonspherical (boomerang) colloids in nematic cells with photopatterned director, J. Phys. Condens. Matter 29 (2017) 014005, doi:10.1088/0953-8984/29/1/014005.

[26] I. Muševič, M. Škarabot, Self-assembly of nematic colloids, Soft Matter 4 (2008) 195–199, doi:10.1039/B714250A.

[27] J.B.;. Fleury, D. Pires, Y. Galerne, Self-connected 3D architecture of microwires, Phys. Rev. Lett. 103 (2009) 267801, doi:10.1103/PhysRevLett.103.267801.

[28] H. Agha, J.B. Fleury, Y. Galerne, Micro-wires self-assembled and 3D-connected with the help of a nematic liquid crystal, Eur. Phys. J. E 35 (2012) 82, doi:10.1140/epje/i2012-12082-1.

[29] N.M. Silvestre, Q. Liu, B. Senyuk, I.I. Smalyukh, M. Tasinkevych, Towards template-assisted assembly of nematic colloids, Phys. Rev. Lett. 112 (2014) 225501, doi:10.1103/PhysRevLett.112.225501.

[30] X. Liu, R. Wei, P.T. Hoang, X. Wang, T. Liu, P. Keller, Reversible and rapid laser actuation of liquid crystalline elastomer micropillars with inclusion of gold nanoparticles, Adv. Funct. Mater. 25 (2015) 3022–3032, doi:10.1002/adfm.201500443.

[31] D. Kasyanyuk, P. Pagliusi, A. Mazzulla, V. Reshetnyak, Y. Reznikov, C. Provenzano, M. Giocondo, M. Vasnetsov, O. Yaroshchuk, G. Cipparrone, Light manipulation of nanoparticles in arrays of topological defects, Sci. Rep. 6 (2016) 20742, doi:10.1038/srep20742.

[32] E. Lee, Y. Xia, R.C. Ferrier, H.N. Kim, M.A. Gharbi, K.J. Stebe, R.D. Kamien, R.J. Composto, S. Yang, Fine golden rings: tunable surface plasmon resonance from assembled nanorods in topological defects of liquid crystals, Adv. Mater 28 (2016) 2731–2736, doi:10.1002/adma.201506084.

[33] M. Wang, Y. Li, H. Yokoyama, Artificial web of disclination lines in nematic liquid crystals, Nat. Commun. 8 (2017) 388, doi:10.1038/s41467-017-00548-x.

[34] K. Sunami, K. Imamura, T. Ouchi, H. Yoshida, M. Ozaki, Shape control of surface-stabilized disclination loops in nematic liquid crystals, Phys. Rev. E 97 (2018) 020701, doi:10.1103/PhysRevE.97.020701.

[35] S. Harkai, B.S. Murray, C. Rosenblatt, S. Kralj, Electric field driven reconfigurable multistable topological defect patterns, Phys. Rev. Res. 2 (2020) 013176, doi:10.1103/PhysRevResearch.2.013176.

[36] X. Wang, D.S. Miller, E. Bukusoglu, J.J.De Pablo, N.L Abbott, Topological defects in liquid crystals as templates for molecular self-assembly, Nat. Mater. 15 (2015) 106–112, doi:10.1038/nmat4421.

[37] Y. Guo, M. Jiang, S. Afghah, C. Peng, R.L.B. Selinger, O.D. Lavrentovich, Q.H. Wei, Photopatterned designer disclination networks in nematic liquid crystals, Adv. Opt. Mater. 9 (2021) 2100181, doi:10.1002/adom.202100181.

[38] M. Jiang, Y. Guo, R.L.B. Selinger, O.D. Lavrentovich, Q.H. Wei, Designing, Generating and reconfiguring disclination interconnects in nematic liquid crystals, Liq Cryst (2023), doi:10.1080/02678292.2023.2208551.

[39] B.S. Murray, R.A. Pelcovits, C. Rosenblatt, Creating arbitrary arrays of two-dimensional topological defects, Phys. Rev. E Stat. Nonlinear Soft Matter Phys. 90 (2014) 052501, doi:10.1103/PhysRevE.90.052501.

[40] M. Kleman, O.D. Lavrentovich, Soft Matter Physics: An Introduction, Springer-Verlag, New York, 2003.

[41] A.J. Ferris, S. Afghah, R.L.B. Selinger, J.V. Selinger, C Rosenblatt, Electric field-induced crossover from 3D to 2D topological defects in a nematic liquid crystal : experimental verification, Soft Matter 16 (2020) 642–650, doi:10.1039/C9SM01733J.

[42] Y. Guo, S. Afghah, J. Xiang, O.D. Lavrentovich, R.L.B. Selinger, Q.H. Wei, Cholesteric liquid crystals in rectangular microchannels: skyrmions and stripes, Soft Matter 12 (2016) 6312–6320, doi:10.1039/C6SM01190J.

[43] R.C. Jones, A new calculus for the treatment of optical systems I. Description and discussion of the calculus, J. Opt. Soc. Am. 31 (1941) 488, doi:10.1364/JOSA.31.000488.

[44] P. Poulin, V. Cabuil, D.A. Weitz, Direct measurement of colloidal forces in an anisotropic solvent, Phys. Rev. Lett. 79 (1997) 4862, doi:10.1103/PhysRevLett.79.4862.

[45] T.C. Lubensky, D. Pettey, N Currier, Topological defects and interactions in nematic emulsions, Phys. Rev. E 57 (1998) 610, doi:10.1103/PhysRevE.57.610.

[46] B.I. Lev, S.B. Chernyshuk, P.M. Tomchuk, H. Yokoyama, Symmetry breaking and interaction of colloidal particles in nematic liquid crystals, Phys. Rev. E 65 (2002) 021709, doi:10.1103/PhysRevE.65.021709.

[47] D. Pires, J.B. Fleury, Y. Galerne, Colloid particles in the interaction field of a disclination line in a nematic phase, Phys. Rev. Lett. 98 (2007) 247801, doi:10.1103/PhysRevLett.98.247801.

[48] J. Fukuda, H. Stark, M. Yoneya, H. Yokoyama, Interaction between two spherical particles in a nematic liquid crystal, Phys. Rev. E 69 (2004) 041706, doi:10.1103/PhysRevE.69.041706.

[49] Chigrinov, V.G.; Kozenkov, V.M.; Kwok, H.S. Photoalignment of Liquid Crystalline Materials: Physics and Applications, Wiley, West Sussex, 2008, 69–96.

[50] J. Jiang, X. Wang, O.I. Akomolafe, W. Tang, Z. Asilehan, K. Ranabhat, R. Zhang, C. Peng, Collective transport and reconfigurable assembly of nematic colloids by light-driven cooperative molecular reorientations, Proc. Natl. Acad. Sci. U. S. A. 120 (2023) e2221718120, doi:10.1037/pnas.2221718120.

Further reading

Y. Guo, High Resolution and High Throughput Photopatterning of Molecular Orientations By Using Plasmonic metamasks, Dissertation, Kent State University, 2017 http://rave.ohiolink.edu/etdc/view?acc_num=kent1505510348651872.